ACS APPLIED MATERIALS & INTERFACES

Research Article

www.acsami.org

High Photoresponse in Hybrid Graphene–Carbon Nanotube Infrared Detectors

Rongtao Lu,* Caleb Christianson, Ben Weintrub, and Judy Z. Wu*

Department of Physics and Astronomy, University of Kansas, Lawrence, Kansas 66045, United States

ABSTRACT: Efficient exciton dissociation is crucial to obtaining high photonic response in photodetectors. This work explores implementation of a novel exciton dissociation mechanism through heterojunctions self-assembled at the graphene/MWCNT (multiwall carbon nanotube) interfaces in graphene/MWCNT nanohybrids. Significantly enhanced near-infrared photoresponsivity by nearly an order of magnitude has been achieved on the graphene/MWCNT nanohybrids as compared to the best achieved so far on carbon nanotube (CNT) only infrared (IR) detectors. This leads to a high detectivity up to 1.5×10^7 cm·Hz$^{1/2}$·W^{-1} in the graphene/MWCNT nanohybrid, which represents a 500% improvement over the best D^* achieved on MWCNT film IR detectors and may be further improved with optimization on the interfacial heterojunctions. This approach of the self-assembly of graphene/CNT nanohybrids provides a pathway toward high-performance and low-cost carbon nanostructure IR detectors.

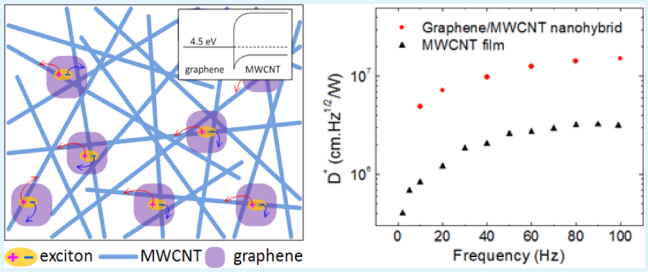

KEYWORDS: *graphene, carbon nanotube, infrared detector, photoresponse*

1. INTRODUCTION

Carbon nanotubes (CNTs) offer a promising alternative to conventional materials for infrared (IR) detection due to their compatible band gap and high absorption coefficient in the IR spectrum.[1] Considerable progress has been made recently using both individual CNTs[2,3] and CNT films[4−10] for IR detections, and a prototype infrared camera was recently reported using a single nanotube photodetector.[11] Recent work on individual CNT employed mechanism of engineering electrode contacts.[3,12] By comparison, CNT films have unique advantages in IR detection in terms of ease of fabrication, low cost, and scalability. This has motivated considerable efforts in the development of CNT film IR detectors of different types including photodiodes,[13,14] photoconductors,[2,8,15] and bolometers.[4,5] In the first two kinds of devices, the incident photogenerated excitons can be dissociated at either the metal−CNT Schottky interface[14] or the heterojunction interfaces between CNT and other appropriately conjugated semiconductors.[15] Consequently, a photocurrent can be observed as photoresponse. For bolometers, the excitons are dissociated to phonons via interaction with lattice, and the dissipated heat induces slow resistance change as bolometric photoresponse.[4,5] Higher figure-of-merit photodetectivity D^* values by 1−2 orders of magnitude were observed on the first two kinds CNT IR detectors[15,16] as compared to that on CNT bolometers,[10] suggesting implementation of efficient exciton dissociation mechanism in CNT films is important toward obtaining high photoresponse in CNT IR detectors. This is anticipated, considering the high exciton binding energy in these one-dimensional systems.[17]

In a recent work, we have demonstrated generation of type-II heterojunctions at the interface of semiconducting SWCNTs and Poly(3-hexylthiophene) (P3HT) nanohybrid IR detectors.[15] The photodetectivity D^* up to 2.3×10^8 cm·Hz$^{1/2}$·W^{-1} was obtained at room temperature, which represents the best so far achieved on CNT-based IR detectors. This result confirms the exciton dissociation mechanism facilitated by the band-edge offset at the type-II heterojunctions indeed plays a critical role in further photoresponse improvement of CNT film IR detectors. Considering the additional steps necessary in separating SWCNTs (i.e., to eliminate the metallic SWCNTs) and in forming the type-II heterojunctions between SWCNT and P3HT, exploration of more robust schemes to incorporate the heterojunction mechanism into MWCNT films is important to large-scale applications of the CNT IR detectors, if an appropriate heterojunction can be formed with other materials.

Graphene may form heterojunctions on CNTs with band-edge offset in a wide range depending on the specific CNT diameter and chirality[18] and the actual contact may also vary greatly by controlling the geometric angular alignment of the atomic lattices.[19] These junctions may form in a robust way on CNT films by simply dispersing graphene flakes into CNT networks. Because the bulk-fabricated CNTs are typically mixtures of CNTs with different chiralities, the graphene/CNT junctions formed with negligible band-edge offsets may not generate any detrimental effects. Instead, they may be beneficial

Received: August 10, 2013
Accepted: October 28, 2013
Published: October 28, 2013

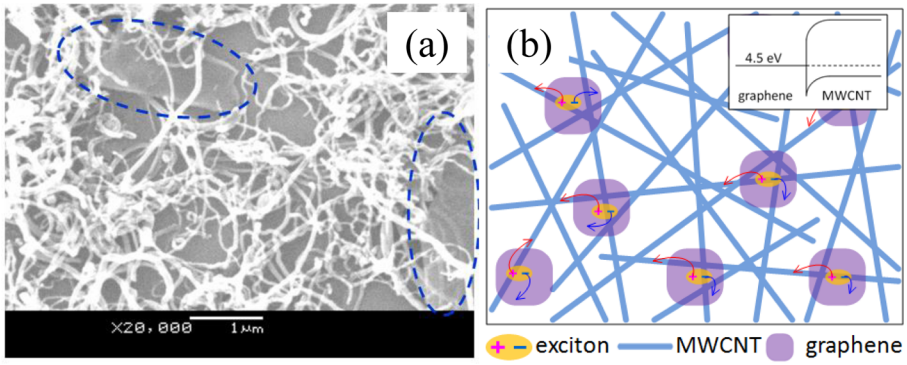

Figure 1. (a) SEM image of graphene/MWCNT nanohybrid. (b) Schematic of exciton dissociation in graphene/MWCNT nanohybrid. The inset shows the band diagram of graphene/MWCNT nanohybrid.

to electron/hole (charge) and phonon (heat) transport if the graphene flakes happen to cover across the intertube junctions, which are regarded as weak links to charge/heat transport in pristine CNT films. The hindered transport across intertube junctions has profound effects on the CNT bolometer performance. First of all, the dominance of large intertube resistance in CNT films over the intratube resistance leads to a lower temperature coefficient of resistance (TCR), which is attributed to the intratube semiconducting transport properties. This argument is supported by the improved photoresponse obtained on thermally annealed CNT films via optimizing the intertube coupling.[20,21] Enhanced detectivity by a factor of 3 due to improved TCR and reduced noise level was observed in annealed MWCNT films as opposed to the original reference samples.[20,21] The dimension of graphene flakes is typically a few micrometers, which is comparable to the length of most CNTs and may be well dispersed over the CNT network in large scales. In this paper, we report the experimental results on fabrication and characterization of self-assembled graphene/CNT nanohybrid film IR detectors, on which significantly improved photoresponse has been demonstrated.

2. EXPERIMENTAL DETAILS

MWCNT with a diameter of 40−60 nm (fabricated by using chemical vapor deposition) was mixed with graphene flakes (5−8 nm thick, XGnP-M-5, XG Sciences[22]) in a mass ratio of 3:1 and then dispersed in deionized water with Triton X-100 surfactant using a bath ultrasonic processor. It should be noted that graphene is a gapless semiconductor and direct measurement on graphene films without asymmetric Schottky contacts yielded negligible photoresponse, and shorts through connections of graphene flakes in the graphene/MWCNT nanohybrid were intentionally avoided by selecting a low mass portion of graphene. The graphene/MWCNT nanohybrid suspension was processed via vacuum filtration, resulting in a mixed graphene/MWCNT film of about 160 nm thick. The control samples of a comparable thickness in the range 200 nm thick reference MWCNT film, without adding graphene, was also fabricated in the same way using pure MWCNT.[10] The films were then transferred onto a Si(100) substrate with a 500 nm thick thermal oxide, which had four Ti(5 nm)/Au(40 nm) electrodes predeposited using electron beam evaporation and was annealed at 400 °C in high vacuum.[10,21] The spacing between two adjacent voltage electrodes is about 0.35 mm, and the width of the samples is about 0.3−0.4 mm. No passivation layer was applyed on the graphene/MWCNT film before measurements. IR radiation was provided by NIR light (1−1.3 μm). The sample was biased using current source, and IR modulation was controlled using a mechanical chopper. Noise was measured using a spectrum analyzer. More details of IR detection measurement setup can be found elsewhere.[5] All measurements were performed in air at room temperature.

3. RESULTS AND DISCUSSION

Figure 1a shows the scanning electron microscopy (SEM) image of the graphene/MWCNT nanohybrid, where graphene flakes distributed uniformly into the MWCNT film can be clearly identified. The thickness of the graphene/MWCNT nanohybrid sample is not very uniform in the small thickness range chosen to maximize the TCR,[4,10,21] which is anticipated because the average thickness of the samples studied in this work is only several times of the component MWCNT diameter. In fact, a similar morphology has been also observed in the reference MWCNT films of comparable thickness. In the SEM image, two graphene flakes of a dimension of about 2 μm can be clearly identified, which cover multiple intertube junctions. The exciton dissociation process is shown in Figure 1b, and the inset shows the band diagram of the graphene/MWCNT nanohybrid, where a work function larger than 4.5 eV is employed for MWCNT with a diameter of several tens of nm.[23] After photons are absorbed by the MWCNT and graphene, excitons may be dissociated at the interface of graphene/MWCNT and charges transport to the graphene and CNT network, contributing additional photoconductivity that due to the bolometric effect from the MWCNT film IR detector. On the other hand, the improved transport over the intertube junction decoration of graphene flakes may lead to enhanced TCR and, therefore, increased bolometric photoconductivity.

To pinpoint these effects quantitatively, the resistance−temperature ($R-T$) curves were taken on a representative graphene/MWCNT nanohybrid sample and a MWCNT reference sample. The resistivity of the graphene/MWCNT nanohybrid is about 0.08 Ω·cm, which is slightly smaller by a factor of 20% than that of ∼0.1 Ω·cm for the reference MWCNT films. This suggests a considerable improvement in electrical transport through the MWCNT network via graphene decoration. On the other hand, the fact that the composite resistivity is not dramatically different from that of the reference MWCNT film is indicative of "no through graphene short" at the selected graphene mass concentration. Figure 2 compares the $R-T$ curves of these two samples with R normalized to its values at room temperature. Both samples show semiconductive $R-T$ behaviors with a monotonic increase of R

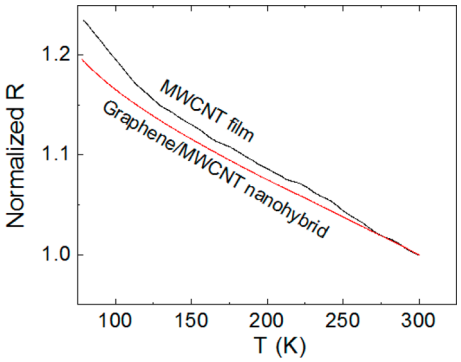

Figure 2. $R-T$ curves of graphene/MWCNT nanohybrid and MWCNT samples.

with decreasing T whereas the graphene/MWCNT nanohybrid has a similar T dependence to the reference sample at higher temperatures in the range 270−300 K but slightly lower T dependence at lower temperatures. At room temperature, the calculated TCR for the graphene/MWCNT nanohybrid is around −0.08%/K and that for the reference MWCNT film is around −0.07%/K.[20] A possibility of this TCR improvement of about 15%, together with the reduced resistivity, is attributed to the improvement of intertube coupling.[21]

Figure 3 shows the temporal response of (a) the graphene/MWCNT nanohybrid in comparison with (b) the reference MWCNT samples to the NIR radiation, which consists of a train of reproducible square-wave pulses corresponding to the 10 Hz incident NIR modulation. The NIR power intensity was about 0.3 mW/mm^2, and the bias current was 2 mA in both cases. A resistance change, $\Delta R/R_0$, around 1.6% observed on the graphene/MWCNT nanohybrid is about 4 times that observed in the reference MWCNT film (∼0.4%),[10] where $\Delta R = R_0 - R_1$; R_1 is the resistance under NIR illumination and R_0 is the initial resistance in dark. This higher $\Delta R/R_0$ value implies higher photoresponse in the graphene/MWCNT nanohybrid. In addition, a significantly improved signal-to-noise ratio was observed on the graphene/MWCNT nanohybrid as opposed to the reference MWCNT samples, which was determined by the higher photoresponse. Considering the graphene flake induced TCR improvement is only on the order of 10%−15%, it is unlikely responsible for the observed large photoresponse enhancement of ∼400%. Instead, the heterojunctions generated at the graphene/MWCNT interfaces may facilitate exciton dissociation in a similar way to the case of SWCNT/P3HT nanohybrids.[24] On the other hand, the response time of the graphene/MWCNT nanohybrid samples is about 1.5 ms, which is in the range of that for reference MWCNT films[10,15] and for the semiconductive SWCNT/P3HT nanohybrids.

Figure 4 compares the voltage responsivity (R_V) as function of (a) bias current and (b) incident NIR source modulation frequency taken on the graphene/MWCNT nanohybrid and the reference MWCNT samples. The R_V is defined as $R_V = \Delta V/\Delta P$, where $\Delta V = I\cdot\Delta R$ is the voltage response, I is the bias current, and ΔP is the NIR power incident to the detection element. The R_V's of the two kinds of the samples qualitatively follow the similar trends as the bias current, and NIR modulation frequencies (f) are varied in the ranges shown in Figure 4.[10] One difference made by graphene flake decoration on the MWCNT network is the higher bias currents above 3 mA the nanohybrid sample could take with R_V not considerably deviating from the R_V vs I trend by extrapolating the curve from the lower bias currents. Increased fluctuation in R_V at higher currents above 2.5 mA was observed in the graphene/MWCNT nanohybrid, which we speculate was caused by heating at higher resistance spots (hot spots) in the MWCNT network at the CNT intertube junctions or/and the graphene/MWCNT interfaces. In contrast, the R_V saturates at $I > 3$ mA for the reference MWCNT sample. This observation provides further support of the improved photoresponse in the graphene/MWCNT nanohybrid via graphene flake decoration. And the almost stable responsivity at different modulation frequencies up to 100 Hz is an expected result of the small response time. Compared with the reference MWCNT sample, the responsivity of the graphene/MWCNT nanohybrid sample is enhanced by more than 8 times at the same bias current and modulation frequency, suggesting a dramatic contribution from heterojunctions formed on the interface between graphene and MWCNTs.

The figure-of-merit detectivity D^* was characterized to further probe the mechanism responsible for the enhanced responsivity. The D^* is expressed as $D^* = R_V (A_d^{(1/2)}/\nu_n)$, where A_d is detection area and ν_n is the noise voltage per bandwidth. Thus, the voltage noise spectra S_V of graphene/MWCNT nanohybrids were first characterized and illustrated in Figure 5a. As the noises in MWCNT films were standard $1/f$ spectra and have been reported,[20] Figure 5a only shows the S_V vs f spectra of the graphene/MWCNT nanohybrid at two different bias currents of 1 and 2 mA, respectively, which are in parallel to the ideal $1/f$ behavior (straight line, red). This indicates the noise behavior in graphene/MWCNT nanohybrids is also $1/f$ type, which is similar to the case of the MWCNT films.[20] The S_V spectra shift up when the bias current is increased and decrease at higher frequencies because $S_V = \nu_n^2$

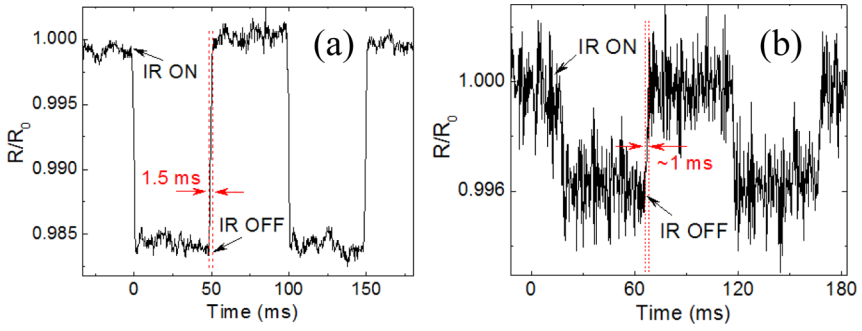

Figure 3. Temporal response of (a) graphene/MWCNT nanohybrid and (b) reference MWCNT film. NIR ∼ 0.3 mW/mm^2, f = 10 Hz. Bias current of 2 mA for both samples.

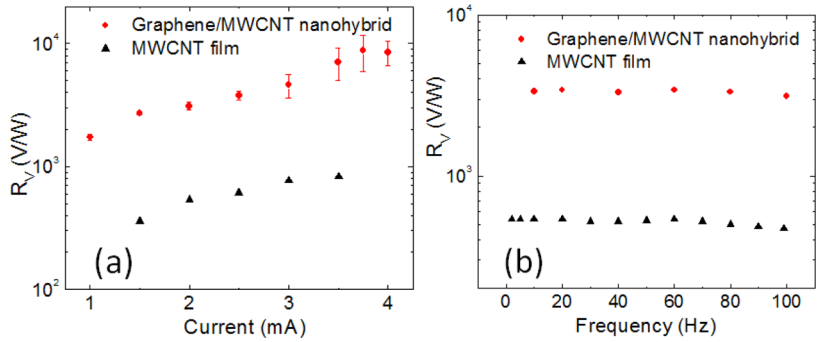

Figure 4. Comparison of R_V as a function of (a) current and (b) frequency for graphene/MWCNT nanohybrid and reference MWCNT film. NIR intensity ~0.3 mW/mm^2 for both figures. A 10 Hz modulation frequency was applied for panel a and a 2 mA bias current was applied for panel b.

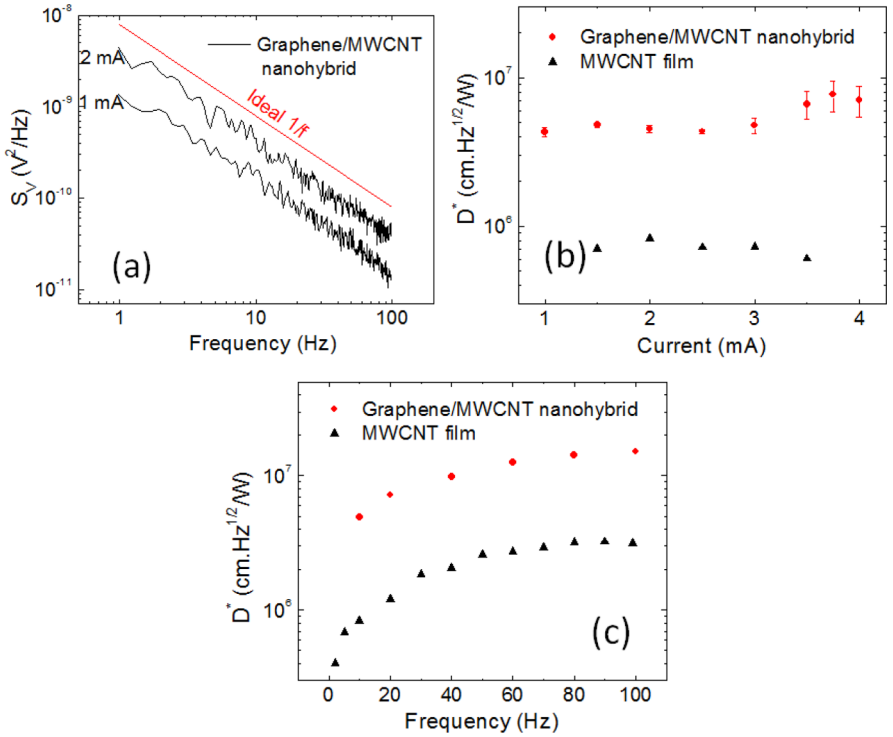

Figure 5. (a) Noise spectrum S_V vs frequency of graphene/MWCNT nanohybrid. The straight line shows ideal $1/f$ performance. (b and c) Comparisons of D^* as a function of (b) bias current and (c) frequency for graphene/MWCNT nanohybrid and reference MWCNT films. NIR intensity ~0.3 mW/mm^2 for both figures. A 10 Hz modulation frequency was used (b), and a 2 mA bias current was used (c).

$= (A_n V^2/f)$ for $1/f$ noise, where A_n is the material's noise amplitude coefficient.[25] The calculated A_n of the graphene/MWCNT nanohybrid is around 5×10^{-11}, which is about 5 times of that of the reference MWCNT film ($\sim 1 \times 10^{-11}$).[20] The increased noise amplitude is not anticipated from the reduced resistivity in graphene/MWCNT nanohybrids with decoration of the graphene flakes on the MWCNT film, indicating the graphene/MWCNT nanohybrid differs from the pure MWCNT reference films considerably. In particular, the role of the graphene flakes is not limited to simply improving the intertube transport of charge and heat. Considering the significantly enhanced photoresponse in the graphene/MWCNT nanohybrids, it is plausible to argue that the heterojunctions formed between graphene flakes and MWCNTs provide additional exciton dissociation mechanism, which may enhance the dark current as well and therefore contribute to noise.

Using the noise voltage v_n obtained in the noise spectra, the D^* is estimated as a function of the bias current I and frequency f, respectively, for the graphene/MWCNT nanohybrid and reference MWCNT samples. The results are shown in Figure 5b,c. In the comparison of D^* vs I curves for these two kinds of samples in Figure 5b, the D^* of the reference MWCNT sample increases slightly with current at lower currents and levels off before falls at higher bias current in exceeding 2.5 mA. In contrast, the D^* for the graphene/MWCNT sample takes an upper turn at higher bias current reaching a peak D^* of 7.6×10^6 cm·Hz$^{1/2}$·W^{-1} at $I \sim 3.75$ mA. The fluctuations in D^* are induced by the fluctuations of R_V shown in Figure 4a. To compare the D^* vs f properties, both samples were biased at 2 mA to avoid the possible damage induced at higher bias currents. As shown in Figure 5c, the D^* vs f curves for both samples have consistent trends that D^* increases with frequency, which is qualitatively determined by the combined variation of R_V and v_n.[5] The maximum D^* obtained on

graphene/MWCNT nanohybrids at a higher frequency of 80−100 Hz is about 1.5×10^7 cm·Hz$^{1/2}$·W^{-1}, which is higher than that of the reference MWCNT sample by a factor of 5. The much improved NIR photoresponse performance in the graphene/MWCNT nanohybrid suggests implementation of exciton dissociation mechanism in CNT films is an important pathway toward enhanced photoresponse and detectivity. It is worth pointing out that the meaurements were stable and repeatable, mainly due to the dominant exciton dissociation mechanism and the stability of component graphene and nanotube. The heterojunctions formed at the interface between graphene and CNTs may be further improved via interface engineering.

4. CONCLUSIONS

We have fabricated graphene/MWCNT nanohybrids by decorating MWCNT networks with graphene flakes. The interfacial heterojunctions formed between graphene and MWCNT have been shown to provide an efficient exciton dissociation mechanism required for high-performance photodetectors. Significantly enhanced photoresponse to NIR radiation was achieved in the graphene/MWCNT nanohybrid IR detectors. This results in an improved figure-of-merit D^* by a factor of 5 to 1.5×10^7 cm·Hz$^{1/2}$·W^{-1} in graphene/MWCNT nanohybrid as compared with the best so far demonstrated on CNT films, in which the bolometric effect dominates the NIR photoresponse. A plausible mechanism is the enhanced exciton dissociation at the interfaces of graphene/MWCNT heterojunctions, which can lead to significantly enhanced photoconductivity. This argument is supported by nearly an order of magnitude increase in responsivity and considerably higher noise amplitude after graphene flake decoration on MWCNT films. In addition, a minor benefit of an improved intertube charge and heat transport is provided with graphene flake decoration on the MWCNT network, it is limited to 10−15% improvement to the bolometric photoresponse as suggested by the observed resistivity reduction and TCR increase. This result suggests that forming heterojunctions between graphene and CNTs can be achieved at a low cost and the self-assembly approach reported in this work may provide a scalable scheme toward high performance IR detectors using carbon nanostructures.

AUTHOR INFORMATION

Corresponding Author

*R. Lu. E-mail: rtlu@ku.edu. J. Wu. E-mail: jwu@ku.edu.

Notes

The authors declare no competing financial interest.

ACKNOWLEDGMENTS

This work was supported in part by ARO (W911NF-12-1-0412) and National Science Foundation (DMR1105986 and EPS-0903806) and matching support from the State of Kansas through Kansas Technology Enterprise Corporation.

REFERENCES

(1) Itkis, M. E.; Niyogi, S.; Meng, M. E.; Hamon, M. A.; Hu, H.; Haddon, R. C. *Nano Lett.* **2002**, *2*, 155−159.
(2) Freitag, M.; Martin, Y.; Misewich, J. A.; Martel, R.; Avouris, P. H. *Nano Lett.* **2003**, *3*, 1067−1071.
(3) Lai, K. W. C.; Xi, N.; Fung, C. K. M.; Chen, H. Optical response time for carbon nanotube based infrared detectors. *9th IEEE Conference on Nanotechnology*, Genoa, 2009.
(4) Itkis, M. E.; Borondics, F.; Yu, A. P.; Haddon, R. C. *Science* **2006**, *312*, 413−416.
(5) Lu, R. T.; Li, Z. Z.; Xu, G. W.; Wu, J. Z. *Appl. Phys. Lett.* **2009**, *94*, 163110.
(6) Xiao, L.; Zhang, Y. Y.; Wang, Y.; Liu, K.; Wang, Z.; Li, T. Y.; Jiang, Z.; Shi, J. P.; Liu, L. A.; Li, Q. Q.; Zhao, Y. G.; Feng, Z. H.; Fan, S. S.; Jiang, K. L. *Nanotechnology* **2011**, *22*, 025502.
(7) Rao, F. B.; Liu, X.; Li, T.; Zhou, Y. X.; Wang, Y. L. *Nanotechnology* **2009**, *20*, 055501.
(8) Levitsky, I. A.; Euler, W. B. *Appl. Phys. Lett.* **2003**, *83*, 1857−1859.
(9) Fujiwara, A.; Matsuoka, Y.; Suematsu, H.; Ogawa, N.; Miyano, K.; Kataura, H.; Maniwa, Y.; Suzuki, S.; Achiba, Y. *Jpn. J. Appl. Phys., Part 2* **2001**, *40*, L1229−L1231.
(10) Lu, R. T.; Shi, J. J.; Baca, F. J.; Wu, J. Z. *J. Appl. Phys.* **2010**, *108*, 084305.
(11) Chen, H. Z.; Xi, N.; Song, B.; Chen, L. L.; Zhao, J. G.; Lai, K. W. C.; Yang, R. G. *IEEE Sens. J.* **2013**, *13*, 949−958.
(12) Yang, L. J.; Wang, S.; Zeng, Q. S.; Zhang, Z. Y.; Pei, T.; Li, Y.; Peng, L. M. *Nat. Photonics* **2011**, *5*, 672−677.
(13) Ong, P. L.; Euler, W. B.; Levitsky, I. A. *Appl. Phys. Lett.* **2010**, *96*, 033106.
(14) Chen, H. Z.; Xi, N.; Lai, K. W. C.; Fung, C. K. M.; Yang, R. G. *IEEE Trans. Nanotechnol.* **2010**, *9*, 582−589.
(15) Lu, R. T.; Christianson, C.; Kirkeminde, A.; Ren, S. Q.; Wu, J. Z. *Nano Lett.* **2012**, *12*, 6244−6249.
(16) Zeng, Q. S.; Wang, S.; Yang, L. J.; Wang, Z. X.; Pei, T.; Zhang, Z. Y.; Peng, L. M.; Zhou, W. W.; Liu, J.; Zhou, W. Y.; Xie, S. S. *Opt. Mater. Express* **2012**, *2*, 839−848.
(17) Wang, F.; Dukovic, G.; Brus, L. E.; Heinz, T. F. *Science* **2005**, *308*, 838−841.
(18) Su, W. S.; Leung, T. C.; Chan, C. T. *Phys. Rev. B* **2007**, *76*, 235413.
(19) Paulson, S.; Helser, A.; Nardelli, M. B.; Taylor, R. M.; Falvo, M.; Superfine, R.; Washburn, S. *Science* **2000**, *290*, 1742−1744.
(20) Lu, R. T.; Kamal, R.; Wu, J. Z. *Nanotechnology* **2011**, *22*, 265503.
(21) Lu, R. T.; Xu, G. W.; Wu, J. Z. *Appl. Phys. Lett.* **2008**, *93*, 213101.
(22) http://www.xgsciences.com/.
(23) Shiraishi, M.; Ata, M. *Carbon* **2001**, *39*, 1913−1917.
(24) Ren, S. Q.; Bernardi, M.; Lunt, R. R.; Bulovic, V.; Grossman, J. C.; Gradecak, S. *Nano Lett.* **2011**, *11*, 5316−5321.
(25) Collins, P. G.; Fuhrer, M. S.; Zettl, A. *Appl. Phys. Lett.* **2000**, *76*, 894−896.